JOURNAL OF MATERIALS SCIENCE **34** (1999) 4031–4037

Sol-Gel derived $SrTiO_3$ and $SrZrO_3$ coatings on SiC and C-fibers

R. WURM, O. DERNOVSEK, P. GREIL*
Department of Materials Science, Glass and Ceramics, University of Erlangen–Nuernberg, Martensstrasse 5, D-91058 Erlangen, Germany
E-mail: greil@ww.uni-erlangen.de

Sols in the systems Sr-Ti-O and Sr-Zr-O have been prepared by an alkoxide sol/gel-process using Strontium acetate, Titanium-isopropoxide and Zirconium-*n*-propoxide. SiC- and C-fibers were coated with the $SrTiO_3$ and $SrZrO_3$ sols. Annealing in N_2-atmosphere at temperatures of 900 and 1100 °C resulted in the formation of crack free coatings of monophase $SrTiO_3$ and $SrZrO_3$, respectively. The thickness of the coatings ranged from 350 to 500 nm. The $SrTiO_3$ and $SrZrO_3$ reaction products were characterized by differential thermal analysis (DTA), thermal gravimetry (TG), X-ray diffraction (XRD) and scanning electron microscopy (SEM).

1. Introduction

Fiber reinforced Ceramic Matrix Composites (CMC) are of particular interest for application under high thermal and mechanical loading conditions such as in aerospace, aircraft, vehicles, electric power generation and high temperature thermal processing. The thermomechanical properties of fiber reinforced ceramics are strongly influenced by the fiber/matrix interface structure [1].

Fiber coatings which generate a controlled fiber/matrix decohesion during interaction with a propagating crack are therefore of particular benefit for increased strength and toughness. Fiber/matrix interface shear strength can be tailored by functional layers [2, 3]. Usually thin coatings of pyrocarbon (PyC) or hex-BN are formed on the fibers by chemical vapour deposition (CVD) [4]. High temperature resistant oxide coatings such as perovskite phases ABO_3 with A = Sr and B = Ti, Zr are of increasing interest for the development of oxidation resistant CMCs [5, 6]. Perovskite phases are of fundamental significance for their electrical and electrooptical properties including ferroelectricity, piezoelectricity but they also offer interesting high temperature properties [7–9]. Some perovskite phases can show extremely high melting point up to 2900 °C, catalytic effects, corrosion resistance, stress induced phase transformation and a thermal expansion coefficient which can be fitted well to a wide range of subtrate materials. The structure dependent properties can be modified in a wide range by the addition of low concentrations of dopants and by forming disordered solid solutions of two or more perovskites [10]. Some properties of perovskite type $SrTiO_3$ and $SrZrO_3$ are shown in Table I. In contrast to nonoxide coating phases a liquid phase coating using low viscous sols of appropriate composition can be used to form perovskite fiber coatings [11]. This work reports on the liquid phase coating of $SrTiO_3$ and $SrZrO_3$ on a SiC and a C-fiber.

2. Experimental

2.1. Sol-preperation

Titanium isopropoxide 96.7% (Alfa GmbH) and Zirconium-*n*-propoxide 76.6% (Hereaus) were dissolved in acetic acid. The volume ratio of Me-alkoxide precursor to acetic acid was 1 : 2. In order to control the degree of hydrolysis of $Ti(OPr)_4$ and $Zr(OPr)_4$ a solution of strontium acetate in acetic acid (96%) was added under constant stirring. The mol ratio of Me-alkoxide precursor to Sr acetate acetic was 1 : 1 and to hydrolysis water was 1 : 2 adjusted by the diluted acetic acid (96%). Adding sodium hydroxide (conc.) to the sol in the system Sr-Zr-O led to a clear sol after stirring for 10 min and increasing the pH-value up to 4.5 to 5. A clear sol in the system Sr-Ti-O was obtained by elevating the temperature to 70 °C after stirring for one hour. Fig. 1 shows the scheme of sol-preparation.

2.2. Fiber coating

A SiC fiber (Nicalon NL 200, Mitsui) and a C-fiber (T300J, Toray Ind.) were coated with the perovskite sols. Table II summarizes the properties of the fibers. To improve wetting, both fibers were desized chemically with acetone. The fibers were drawn out vertically from the sol having a viscosity in the range of $\eta = 1$–10 mPa·s, with a withdrawal speed in the range of $v = 1$–10 cm·min^{-1}. Drying of the coated fiber was carried out at room temperature in air, followed by calcination under flowing nitrogen at several temperatures, below 1100 °C. Table II summarizes the materials data of the fibers.

* Author to whom all correspondence should be addressed.

TABLE I Properties of perovskite type $SrTiO_3$ and $SrZrO_3$

Perovskite	$SrTiO_3$	$SrZrO_3$
Structure	cubic	orthorombic
Lattice constant (1×10^{-10} m)	*a*, 3.904	*a*, 5.792 *b*, 8.218 *c*, 5.818
Thermal expansion coefficient (RT – 1000 °C) ($10^{-6} \cdot K^{-1}$)	8.6	9.6
Melting temperature (°C)	2083	2899
Density ($g \cdot cm^{-3}$)	5.12	5.46

TABLE II Material data of the C- and SiC-fibers

Properties	C-fiber (T300J, Toray Ind.)	SiC-fiber (Nicalon NL 200, Mitsui)
Fiber diameter (μm)	7.1	14
Number of filaments	3000	500
Tensile modulus (GPa)	239	200
Tensile strength (GPa)	4.3	3.0
Elongation (%)	1.81	1.4
Density ($g \cdot cm^{-3}$)	1.79	2.55
Thermal expansion coefficient (II) ($10^{-6} \cdot K^{-1}$)	0.3	3.1

2.3. Characterisation methods

FT-IR spectra were recorded using a Nicolet Magna-IR-spectrometer (Nicolet, Madison, USA). Sols were deposited on Si-wafer for measurement. For examination of the calcination products the KBr-method (3 mg powder : 300 mg KBr) was applied. The sol-gel transformation was recorded using an oscillating Bohlin CSM cone/plate viscosimeter (Bohlin Ind., Mühlacker, Germany) with a frequency of $f = 1$ Hz (or s^{-1}). Densities of the dried gel and calcined powder were measured by an He-pyknometer Micromeritics Ind., Typ Accupyc 1330 (Micromeritics, Norcross GA, USA). X-ray diffraction was performed on samples deposited on single-crystal Si-wafers using a Siemens Diffrac 5000 diffractometer (Siemens, Karlsruhe, Germany) with CuK_α radiation (40 kV, 30 mA) in a two theta range between 20° and 70°. Thermogravimetric (TG) analysis was carried out in thermal balance, Netzsch STA 409 (Netzsch Gerätetechnik, Selb, Germany) under flowing nitrogen of 100 $cm^3 \cdot min^{-1}$. The fiber coatings were analyzed using SEM. Micrographs were obtained with a Cambridge Instruments Stereoscan 250MK3 (Sterescan MK.II., Cambridge, GB) device. A Link Analytik An 1055 was used for element analysis. For the measurement of the coating layer thickness the fibers were fixed on metal pads and sputtered with gold.

3. Results and discussion

3.1. Sol/gel-transformation

Fig. 2 show FT-IR spectra of a Sr-Ti-O and a Sr-Zr-O fresh sol and the corresponding gel dried at 200 °C in air. Table III summarizes the characteristic wavelengths of the functional groups which are involved in the sol-gel transformation reaction. The main reactions occurring during the sol-gel-transformation are hydrolysis and polycondensation. Hydrolysis of Ti- and Zr-precursor is indicated by characteristic OH-vibrations in the region of 3700–3300 cm^{-1} [12, 13]. Stretching vibrations in the region of 600–700 cm^{-1} are typical for metal-oxygen Sr-O, Ti-O and Zr-O groups. Intensity

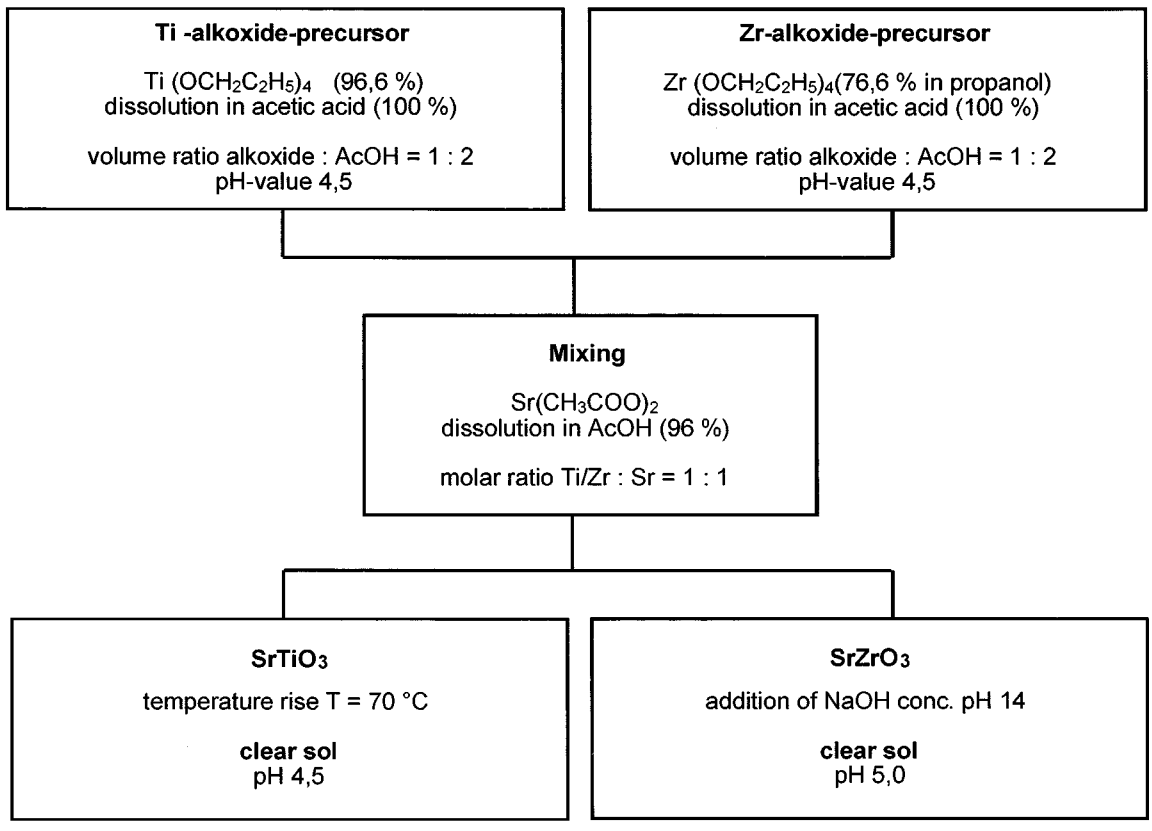

Figure 1 Sol preparation in the system Sr-Ti-O and Sr-Zr-O.

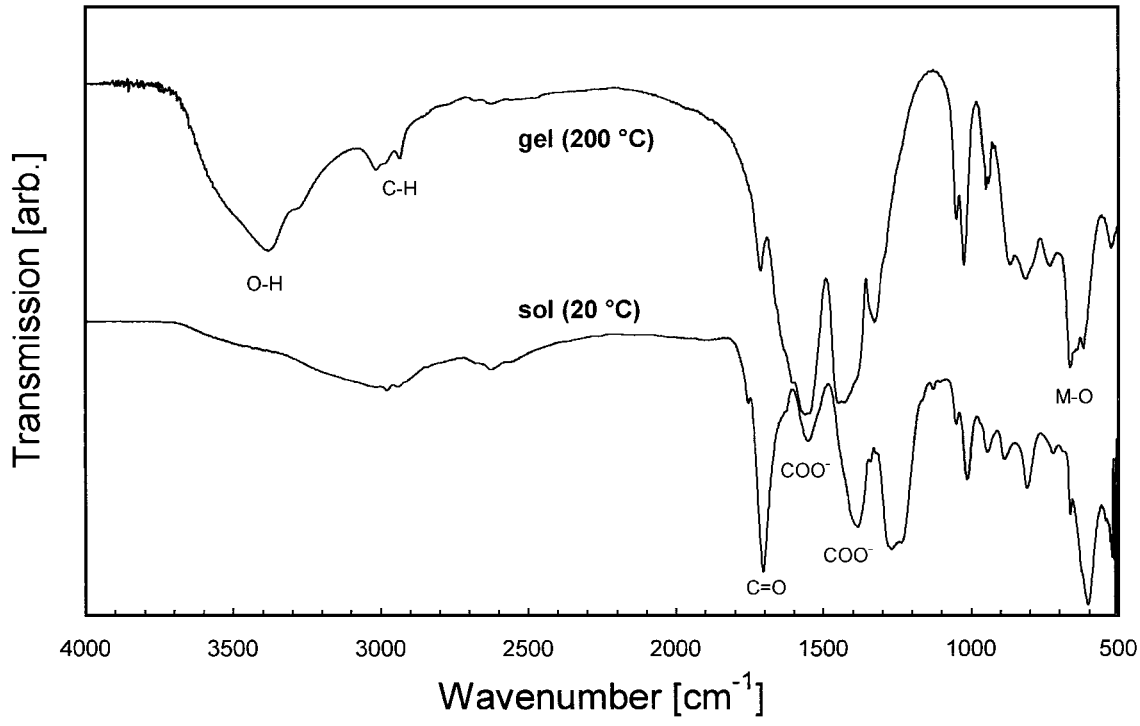

(a)

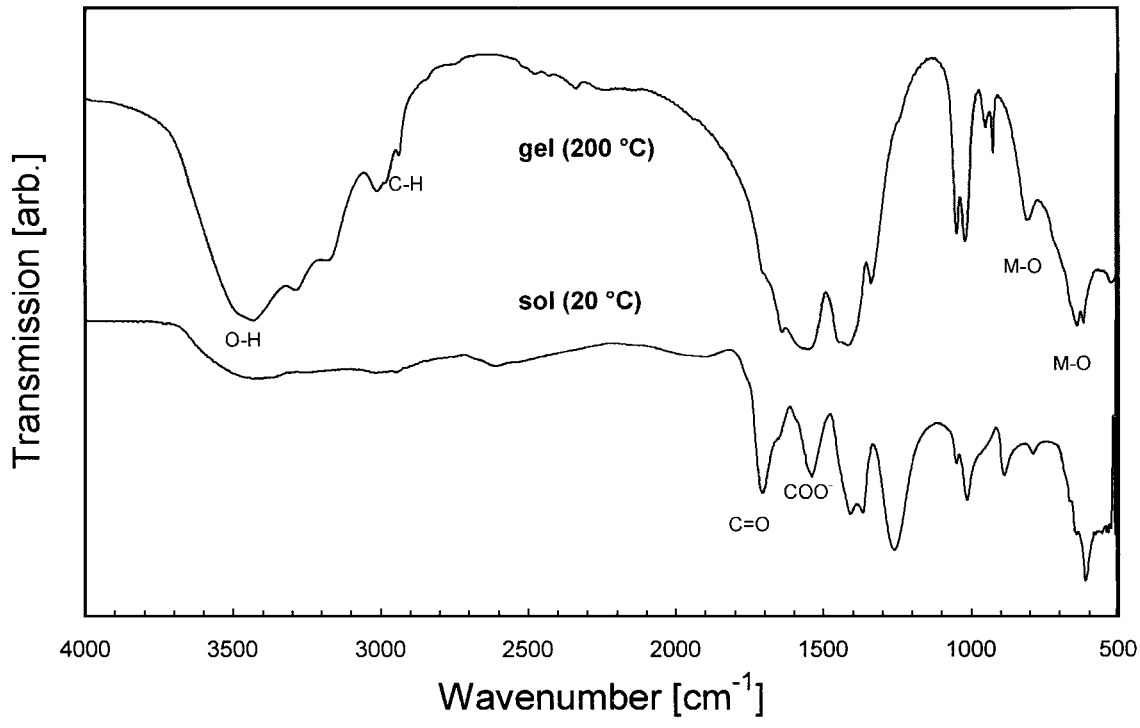

(b)

Figure 2 IR-spectra in the system Sr-Ti-O (a) and Sr-Zr-O (b).

decrease of the stretching at 1700 cm^{-1} of C═O and at 1550 and 1400 cm^{-1} of COO^- indicates disappearance of the solvent acetic acid. Zr- and Ti-gels show the existence of small amounts of COO^- groups retained on isolated $Sr(Ac)_2$. In agreement with infrared spectra the gelation of the Ti- and Zr-precursors involves the formation of [M-OH] and [M-OAc] groups and release of [R-OH] according to

$$M(OR)_4 + yH_2O + zAc(OH) \longleftrightarrow M(OH)_x \cdot (OR)_y \cdot (OAc)_z + (4-y)R\text{-}OH \quad (1)$$

with $x + y + z = 4$.

TABLE III IR-data with the characteristic wavenumber of the functional groups

Functional group	Wavenumber (cm^{-1})
$CH\text{-}CH_2$, CH_3	2970, 2930
C═O	1700
COO^-	1550, 1400
OH	3700–3300
M-O	600–700

3.2. Calcination

Fig. 3a shows X-ray diffraction patterns of the Sr-Ti-O system after annealing of the dried gel at 200, 400,

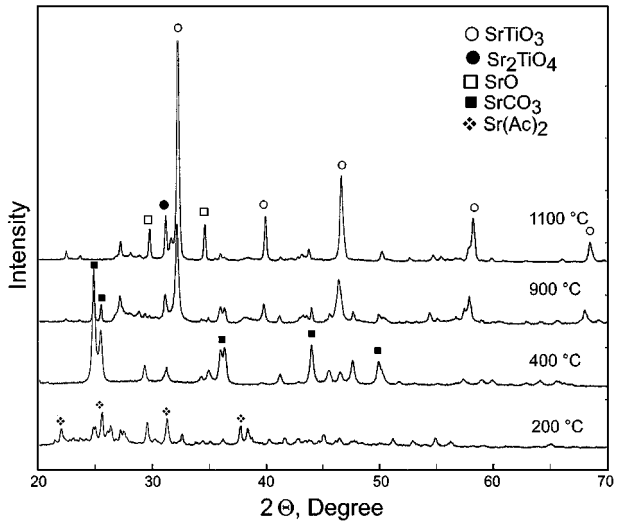

(a)

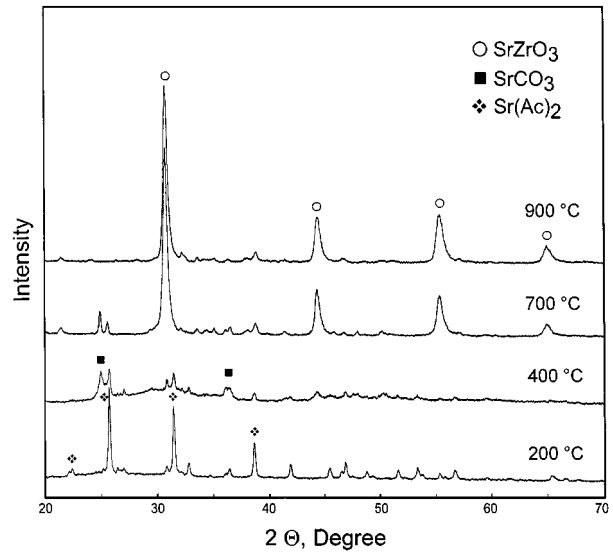

(b)

Figure 3 X-ray spectra of the system Sr-Ti-O (a) and Sr-Zr-O (b) calcinated at different temperatures in N_2-atmosphere.

900 and 1100 °C. While at 200 °C only $Sr(Ac)_2$ is formed, crystalline $SrCO_3$ appears at 400 °C indicating the transformation of the strontium acetate into strontium carbonate,

$$Sr(CH_3COO)_2 \xrightarrow{400\,^\circ C} SrCO_3 + H_3CCOCH_3 \qquad (2)$$

which at higher temperatures has reacted to form $SrTiO_3$.

$$SrCO_3 + TiO_2 \xrightarrow{>400\,^\circ C} SrTiO_3 + CO_2 \qquad (3)$$

At 1100 °C $SrTiO_3$ is the major phase with traces of residual Sr_2TiO_4 and SrO from calcination. In agreement with Pfaff, the formation of Sr_2TiO_4 phase can be explained by a strontium to titanium *ratio* > 1 [14], where SrO is formed by decomposition of $SrCO_3$ above 900 °C.

$$2SrCO_3 + TiO_2 \xrightarrow{900\,^\circ C} Sr_2TiO_4 + 2CO_2 \qquad (4)$$

$$SrCO_3 \xrightarrow{>900\,^\circ C} SrO + CO_2 \qquad (5)$$

Fig. 3b shows X-ray patterns of the Sr-Zr-O gel after annealing at 200, 400, 700 and 900 °C in N_2-atmosphere. Crystallization of $SrZrO_3$ starts between 400 and 700 °C according to

$$SrCO_3 + ZrO_2 \xrightarrow{>400\,^\circ C} SrZrO_3 + CO_2 \qquad (6)$$

At 700 °C no residual $SrCO_3$ is detected and a single phase $SrZrO_3$ is formed. Fig. 4 shows the thermogravimetric analysis of the Sr-Ti- and Sr-Zr-gels dried at 200 °C during heating up to 1100 °C. The $SrTiO_3$ gel has a major weight loss between 130 and 370 °C where evaporation of propanol and the decomposition of the acetic acid takes place. Between 370 and 630 °C the $SrCO_3$ phase remains stable. Above 630 °C decomposition of $SrCO_3$ occurs and finally $SrTiO_3$ is formed. The density increases from 1.97 g·cm^3 at 200 °C (dried gel) up to 4.15 g·cm^{-3} at 1100 °C, which is 80% of the theoretical value of $SrTiO_3$ (5.12 g·cm^{-3}). The Sr-Zr-system shows a similar behavior resulting in a density of 4.68 g·cm^{-3} of the $SrZrO_3$, which is 86% of the theoretical value of $SrZrO_3$ (5.46 g·cm^{-3}). The total weight loss at 1100 °C attains 69% in the Sr-Ti-O and 81% in the Sr-Zr-O-system.

3.3. Fiber coating

The most significant variables which affect fiber coating are the microstructure of the coating, the thickness, and the interfacial shear strength [3, 15]. The thickness λ of the coating layers varies with the fiber withdrawal speed v, the surface roughness of the fibers, the density ρ and viscosity η of the sol [16–18]. The layer thickness λ_{sol} can be estimated in a first approximation by

$$\lambda_{sol} = k\left[\frac{\eta \cdot v}{\rho \cdot g}\right]^{1/2} \qquad (7)$$

where g is the acceleration due the gravity (9.806 m·s^{-2}) and k is a correction factor ($k = 0.1$). The viscosities η of the Sr-Ti-O and the Sr-Zr-O systems were adjusted by acetic acid to 4 and 8 mPas, respectively. Assuming all shrinkage during calcination occurs perpendicular to the fiber surface radial shrinkage ε_r can be expressed as

$$\varepsilon_r = \frac{\Delta\lambda}{\lambda_{sol}} = \frac{\lambda_{cer} - \lambda_{sol}}{\lambda_{sol}} = \frac{\lambda_{cer}}{\lambda_{sol}} - 1 \qquad (8)$$

and for the thickness of the calcined ceramic coating layer λ_{cer}

$$\lambda_{cer} = \left[r^2 + \alpha\beta\left(\lambda_{sol}^2 + 2r\lambda_{sol}\right)\right]^{1/2} - r \qquad (9)$$

r is the radius e.g. 3.5 μm for C and 7 μm for SiC fibers, respectively. α and β desribe the weight and density ratios of the sol and ceramic phases

$$\alpha = \left(\frac{m}{m_{sol}} = \frac{\Delta m}{m_{sol}} + 1\right)$$

and (10)

$$\beta = \left(\frac{\rho_{sol}}{\rho_{cer}} = \frac{\Delta\rho}{\rho_{sol}} + 1\right)^{-1}$$

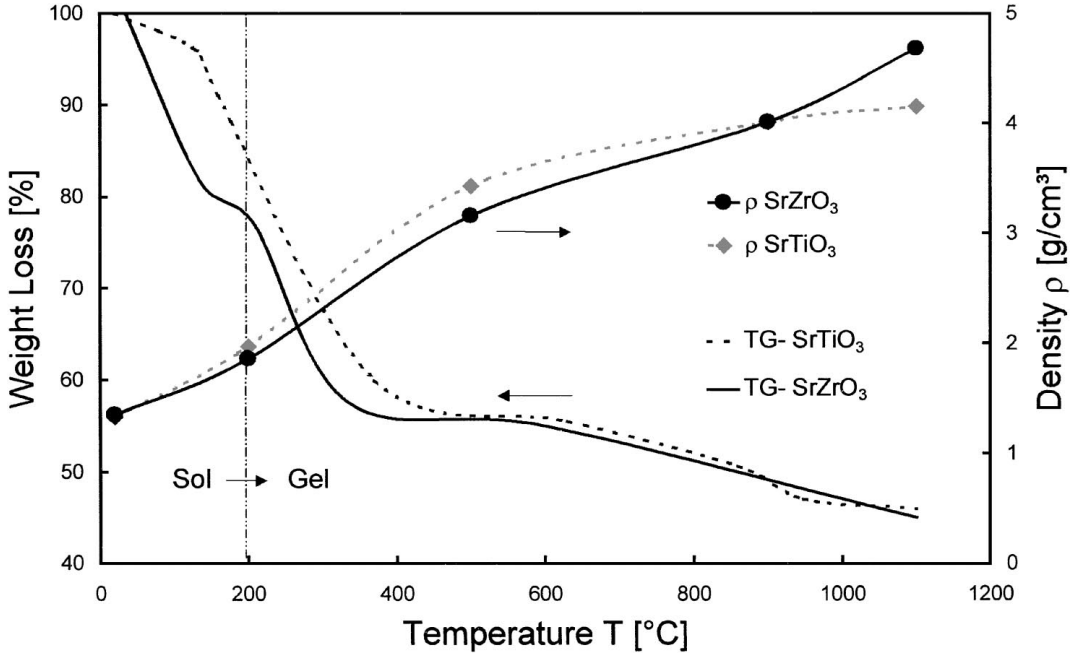

Figure 4 Thermogravimetric analysis and density evolution of the Sr-Ti-O and Sr-Zr-O up to 1100 °C in N_2-atmosphere.

Taking into account the density change from the sol ($\rho_{sol} = 1.33$ g·cm^{-3} Sr-Ti-O and 1.35 g·cm^{-3} Sr-Zr-O) to the perovskite phases (Table I) and the weight change during calcination ($\Delta m/m_{sol} = 0.69$ for Sr-Ti-O and 0.80 for Sr-Zr-O) values for α (0.3099 and 0.1999) and β (0.2596 and 0.2472) for the Sr-Ti-O and the Sr-Zr-O systems were derived. Fig. 5 shows λ_{cer} calculated according to Equation 9 as a function of withdrawal speed v for C-fiber (Similar results for λ_{cer} were obtained for SiC-fiber). The experimental variables are given in Table IV.

The calculations show, that for an experimental $v = 1.6 \times 10^{-3}$ m·s^{-1} a layer thickness λ_{cer} in the range of 300–400 nm results which is confirmed by the SEM analyses of the coating layer thickness. Fig. 6 shows SiC and C-fibers coated with $SrTiO_3$ and $SrZrO_3$. The coatings are almost defect free and no cracks can be observed. Due to the differences in thermal expansion,

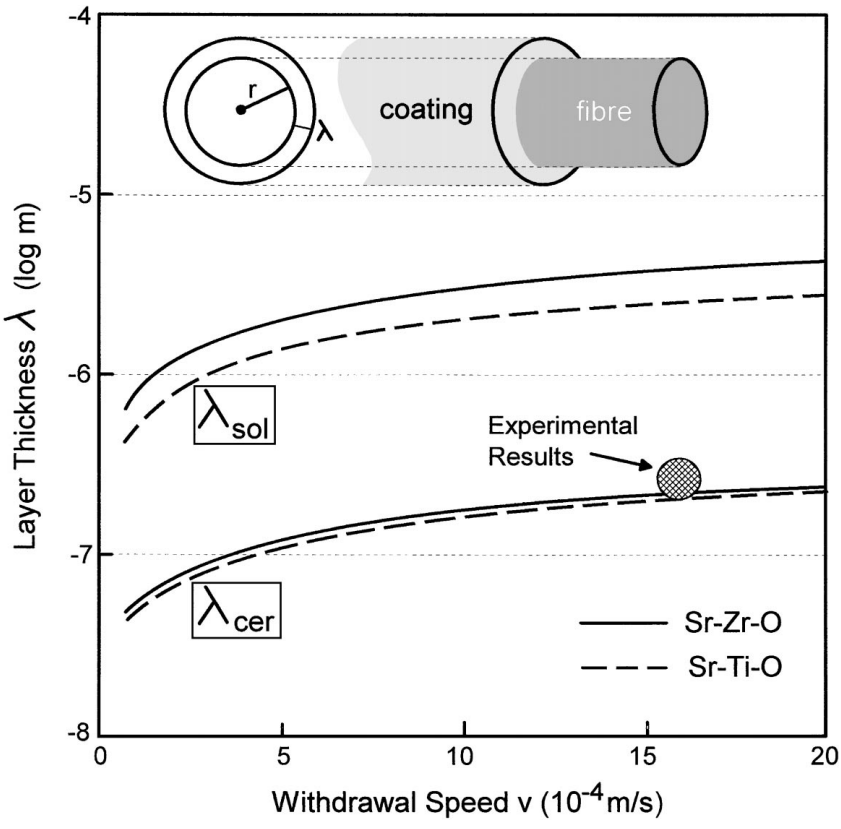

Figure 5 Calculated layer thickness λ_{cer} of $SrTiO_3$ and $SrZrO_3$-coating on C-fiber.

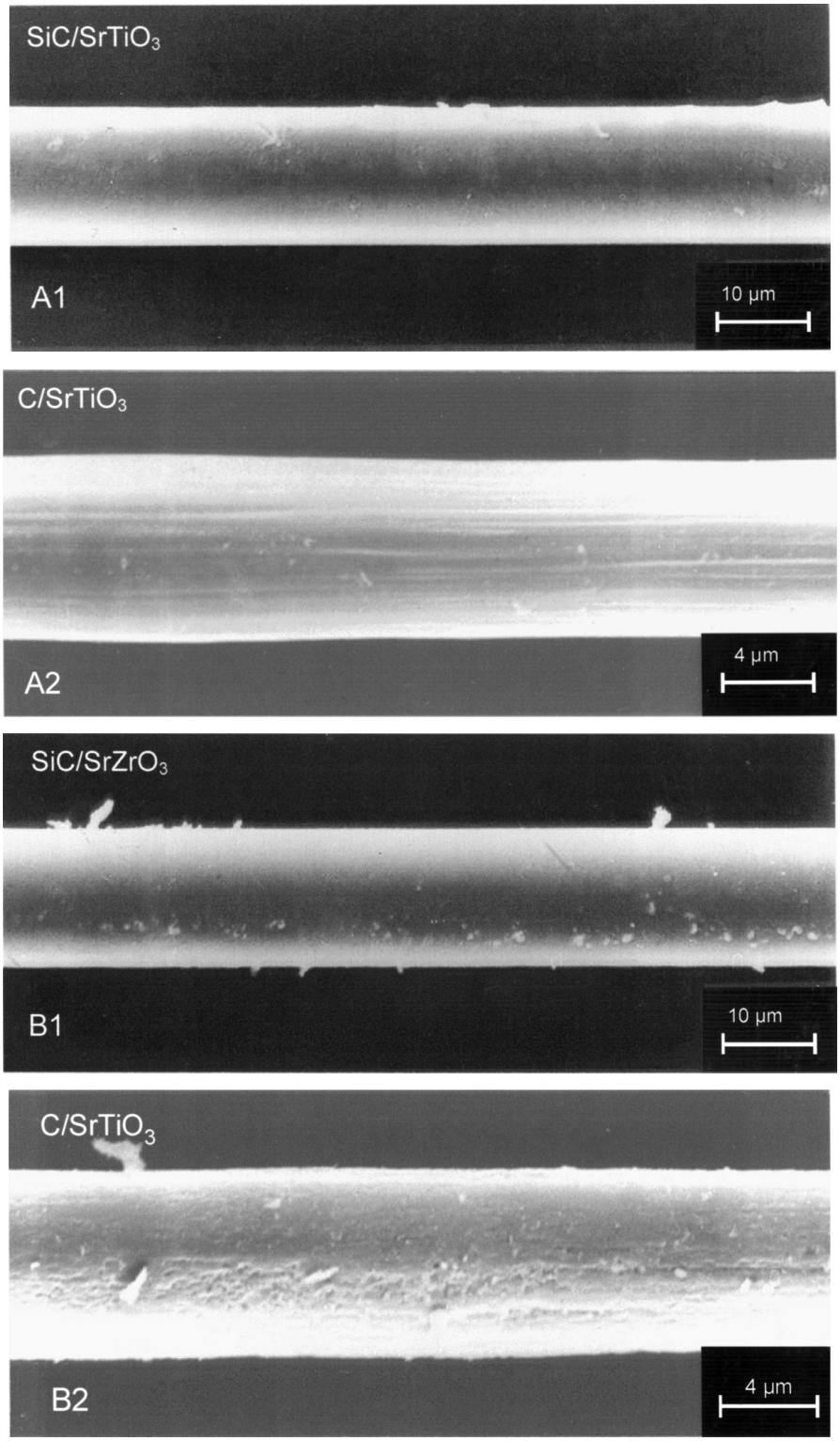

Figure 6 SiC and C-fibers coated with $SrTiO_3$ (A1, A2) and $SrZrO_3$ (B1, B2) at 1100 °C in N_2 atmosphere.

Tables I and II, defect free coating layer are limited by a maximum thickness of approximately 500 nm.

4. Conclusions

Coating layers of the perovskite phases $SrTiO_3$ and $SrZrO_3$ were deposited on SiC- and C-fibers by a liquid phase coating process. Strontium acetate, Titanium propoxide and Zirconium propoxide were used to form a low viscous sol. After coating and annealing in nitrogen atmosphere at 1100 °C the perovskite phases are formed. Crack-free coatings could be obtained up to a maximum thickness of 500 nm. The perovskite coatings are stable in an oxidation environment up to high temperatures and are therefore of particular interest for the development of oxidation resistant CMC.

References

1. A. G. EVANS and F. W. ZOK, *J. Mater. Sci.* **29** (1994) 3857–3896.
2. F. LAMOUROUX, X. BOURRAT and R. NASLAIN, *Carbon* **31**(8) (1993) 1273–1288.

3. R. NASLAIN, The Concept of Layered Interphases in SiC/SiC, in High-Temperature Ceramic-Matrix Composites I: Design, Durability and Performance, edited by A. G. Evans and R. Naslain, *Ceramic Transactions* **57** (1996) 23–39.
4. S. KUMARIA and R. N. SINGH, *J. Amer. Ceram. Soc.* **79**(1) (1996) 199–208.
5. J. CHANT, *J. Mater. Sci.* **30** (1995) 2769–2784.
6. M. KAMALASAN, K. N. DEEPAK and S. CHANDRA, *J. Appl. Phys.* **76** (1994) 4603–4609.
7. B. WECHSLER and K. KIRBY, *J. Amer. Ceram. Soc.* **75**(4) (1992) 981–984.
8. A. B. SCHÄUFELE and K. H. HÄRDT, *ibid.* **79**(10) (1996) 2637–2640.
9. I. BURN and S. NEIRMAN, *J. Mater. Sci.* **17** (1982) 3510–3524.
10. G. PFAFF, *Journal of Experimental and Industrial Crystallography* **26** (1991) 123–130.
11. M. GUGLIELMI and G. CARTURAN, *J. Non-Cryst. Solids* **100** (1988) 16–30.
12. M. KAMALASAN, N. DEEPAK KUMAR and S. CHANDRA, *J. Mater. Sci.* **31** (1996) 2741–2745.
13. E. LEITE, C. M. G. SOUSA, E. LONGO and J. A. VARELA, *Ceramics International* **21** (1995) 143–152.
14. P. PFAFF, *J. Mater. Chem.* **3** (1993) 721–724.
15. S. UEDA, *Mater. Res. Bull.* **9** (1974) 469–476.
16. A. HURD and J. BRINKER, *Mater. Res. Soc. Proc.* **121** (1988) 731–742.
17. L. SCRIVEN, *ibid.* **121** (1988) 717–729.
18. C. BRINKER, A. HURD, G. FREY, K. WARD and C. ASHLEY, *J. Non-Cryst. Solids* **121** (1990) 294–302.

Received 10 March 1998
and accepted 29 January 1999